Supplementary materials
Morphology-Induced Spectral Modification of Self-Assembled WS_2 Pyramids

Irina Komen, Sabrya E. van Heijst, Sonia Conesa-Boj, and L. Kuipers
Kavli Institute of Nanoscience, Department of Quantum Nanoscience, Delft University of Technology, The Netherlands
(Dated: September 22, 2021)

I. WS_2 HOLLOW PYRAMID SAMPLE

Figure 1a presents a wide-field optical image of a part of the sample. Under these growth conditions both hollow pyramids (red), monolayer flakes (green) and full pyramids (blue) are created. Note that there are many hollow pyramids with a comparable size to the one studied in this work (15 μm). Using the same CVD growing conditions (see Methods) yields similar samples with the same distribution of pyramid-like structures.

To provide better insight in the morphology of the hollow WS_2 pyramids, Fig.1b,c depict higher magnification SEM images of the hollow pyramid depicted in Fig.1a in the main text. The black triangle in the middle of Fig.1b is the bottom of the pyramid crater. The top rim can also be distinguished around the crater triangle. The steps of the stair-like sides can clearly be recognized in Fig.1c.

In addition, Transmission Electron Microscopy (TEM) measurements are performed to gain access to the atomic structure of the hollow pyramids. Figure 2a and 2b display low-magnification annular dark-field (ADF) scanning transmission electron microscopy (STEM) images of the side of a hollow WS_2 pyramid. The variations in the contrast visualise clearly the step-like nature of the hollow pyramid side. Figure 2c presents an atomic-resolution ADF-STEM image corresponding to the side of the pyramid. Each bright spot corresponds to an atomic column that is composed of alternating tungsten (W) and sulfur (S) atoms. Using an ADF linescan, extracted from the atomic resolution image across six lattice points, we confirm that the WS_2 within the hollow pyramid crystallizes in a 3R crystal phase (see Fig.2d).

II. SPECTRAL BACKGROUND

The hollow pyramid spectra exhibit a number of Raman modes plus a background (see Fig.3, Fig.6 in the main text). Using the temperature-dependent spectral position of this background, we can explain its origin. Figure 3 depicts the spectral response of the hollow pyramid upon a 595 nm excitation (orange) and a 561 nm excitation (green), comparing this with the photoluminescence of a monolayer exciton (black dotted line). The spectral response of the hollow pyramid to a 595 nm excitation exhibits a background under the higher order Raman modes, whereas the spectral response of a 561 nm excitation exhibits a background separated from the Raman modes, that overlap spectrally (see Fig.3c-d). The spectral position of the photoluminescence peak is completely different (610 - 630 nm in the temperature range 4 K - 300 K). Figure 3e depicts the spectral position of the pyramid background, determined from the spectra of 561 nm excitation (in green), and the spectral position of the exciton PL (black dotted line). Both the pyramid background and the exciton PL peak are blue-shifting with decreasing temperature, however their spectral position is different from each other. At room temperature (Fig.3a), the spectral position of the PL peak (at 630 nm) is very close to the background of the pyramid spectra acquired with a 595 nm excitation (around 645 nm). At 4 K (Fig.3d), the PL peak (at 615 nm) overlaps roughly with the first few Raman features of the pyramid spectra acquired with a 595 nm excitation (around 620 nm). However, at 200 K and especially 100 K (Fig.3b,c), the PL peak overlaps neither with the first Raman features nor the background of the pyramid spectra acquired with a 595 nm excitation. Therefore we conclude that the background of the hollow pyramid spectra is not photoluminescence from the direct bandgap of WS_2.

Another potential explanation for the background in the pyramid spectra is emission from the indirect bandgap. Few-layer WS_2 samples exhibit a combination of direct and indirect bandgap emission [1]. Figure 3f compares the room-temperature spectra of a WS_2 trilayer (grey) and five WS_2 layers (blue) (exfoliated on a Si substrate) with a spectrum from the hollow WS_2 pyramid. The room-temperature spectral position of the indirect bandgap ranges from 700 nm for a bilayer to 850 nm for multilayers [2]. This constitutes a large spectral separation with the measured spectrum (compare Fig.3a). Moreover, with decreasing temperature, the indirect bandgap is reported to exhibit a red shift, *i.e.*, away from the exciton position [3, 4], whereas the pyramid background exhibits a similar blue shift to the exciton PL (see Fig.3e).

An alternative explanation would be emission from a charged exciton or trion. However, the reported spectral position of the trion lies closer to the exciton than the background in the hollow pyramid spectra [5, 6]. We conclude that this background originates in intermediate gap states or defect states, that are reported to be in a range of spectral positions further away from the exciton PL than the trion [6–8], but closer than the indirect bandgap [2–4].

It is interesting to note that the spectral background from these intermediate gap states is more present in the pyramid crater than on the pyramid sides. We propose this might be originated in the higher density of crystallographic defects.

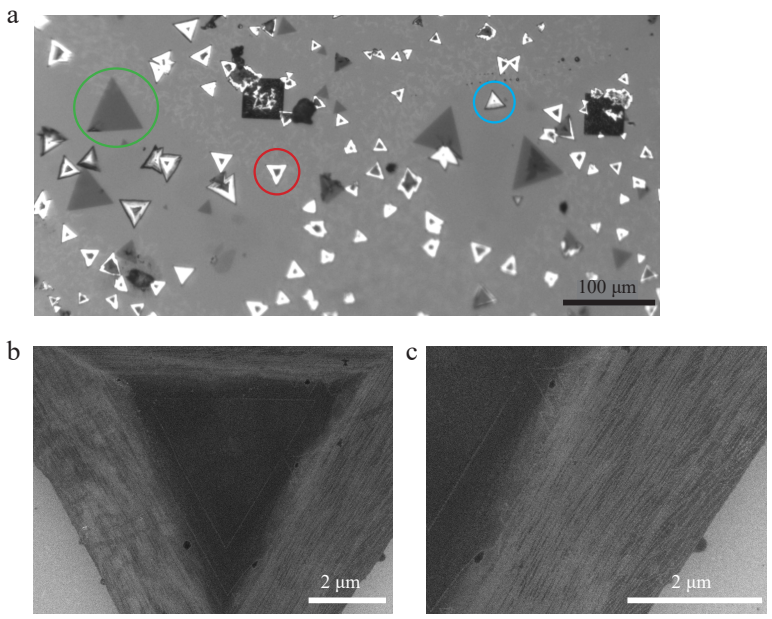

FIG. 1. **Hollow WS_2 pyramid sample**
a. Wide-field optical image of a part of the sample, with hollow pyramids (red), WS_2 monolayer flakes (green) and full pyramids (blue). The black squares are windows in the silicon frame over which a silicon nitride film is spanned (see Methods). Under these growth conditions, many hollow pyramids arise size 10 - 25 μm, comparable to the one presented in this work. **b,c.** SEM images of the hollow WS_2 pyramid studied in the main text. In **b**, the black triangle in the middle is the bottom of the pyramid crater. The top rim of the pyramid can also be distinguished around the triangle of the pyramid crater. The steps in the stair-like sides can be easily recognized in **c**.

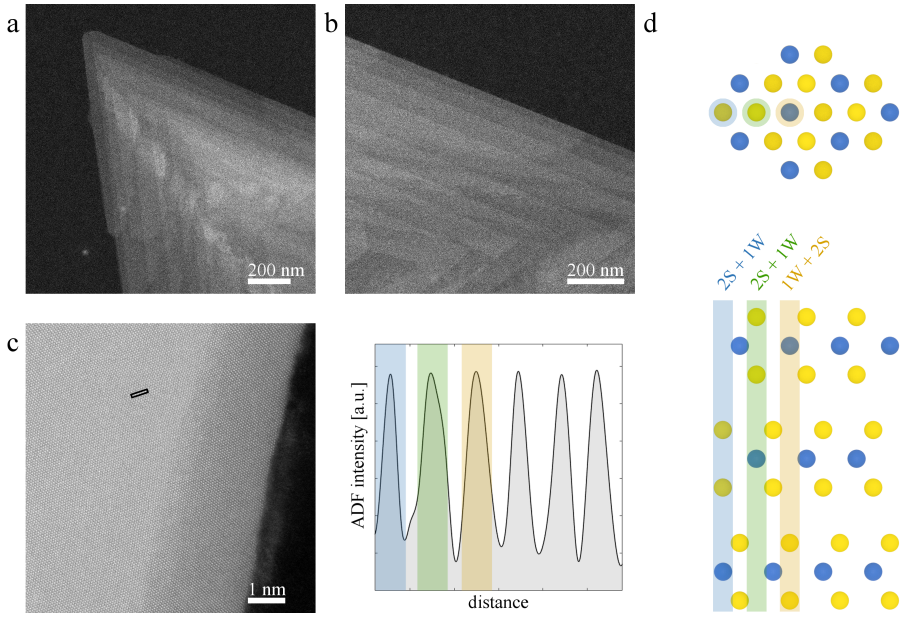

FIG. 2. **Morphology and crystal structure of the hollow WS_2 pyramids**
a-b. Low-magnification ADF-STEM images of a hollow WS_2 pyramid. The step-like nature of the pyramid side is clearly visible by the changes in contrast with every step. **c.** Atomic resolution image corresponding to the side of the hollow pyramid (left panel) and the ADF intensity profile (right panel) acquired along the black outlines region in the atomic resolution image. **d.** Schematic atomic model of the top-view (upper panel) and side-view (lower) of the crystalline structure associated to the 3R-WS_2 phase.

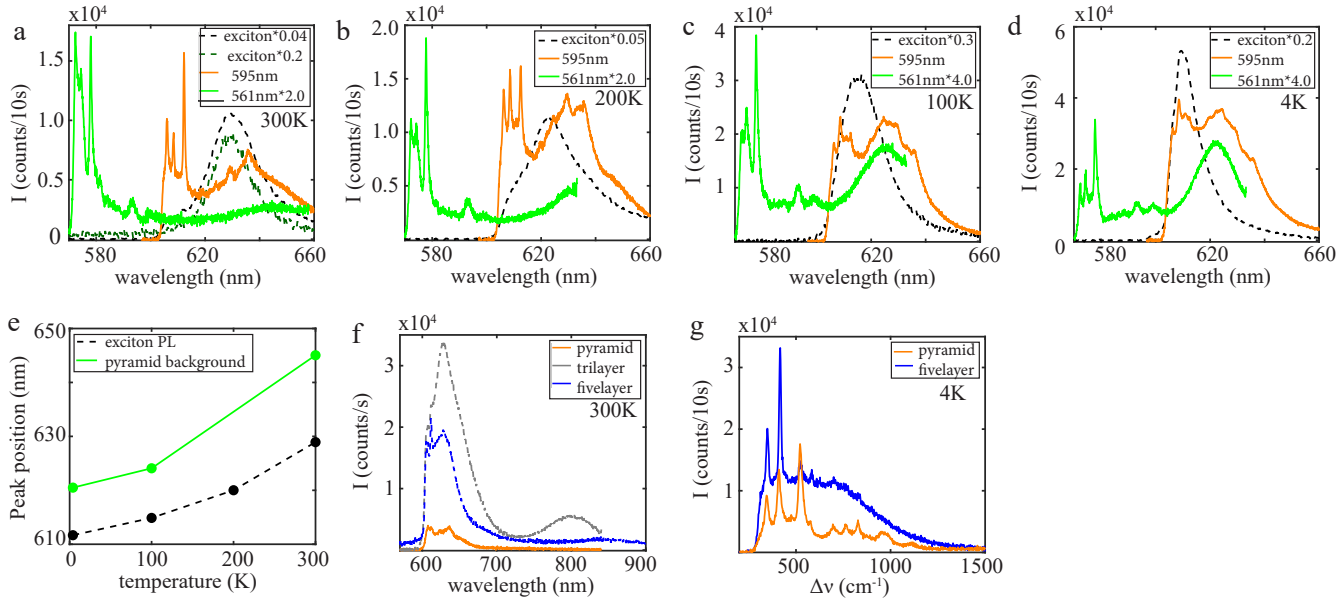

FIG. 3. **Comparison pyramid, monolayer and few-layer spectra**
a-d. Spectral response of a pyramid upon a 595 nm excitation (orange) and a 561 nm excitation (green), and the spectral response of a monolayer upon 595 nm excitation (black dotted line), at temperatures between room temperature and 4 K (the spectra are re-scaled for easier comparison, see legends). The spectral response of the monolayer upon a 561 nm excitation (green dotted line in **a**) has a lower intensity than to the 595 nm excitation, but is at the same wavelength. **e.** The background under the higher order Raman features in the spectra of the 595 nm excitation, and the spectral position of the exciton PL are both blue-shifting with decreasing temperature. **f.** In contrast to the spectra of a WS_2 trilayer (in grey) and five layers of WS_2 (in blue) (exfoliated on a Si substrate), the spectrum of the WS_2 pyramid (in orange) does not exhibit light from an indirect bandgap at 800 - 850 nm wavelength. Moreover, although reduced with respect to the monolayer, the PL from the direct bandgap of the few-layers of WS_2 is clearly distinguishable from the background. **g.** Comparison of the spectral response of the hollow pyramid (in orange) and of five layers of WS_2 (in blue), acquired at 4 K with a 595 excitation.

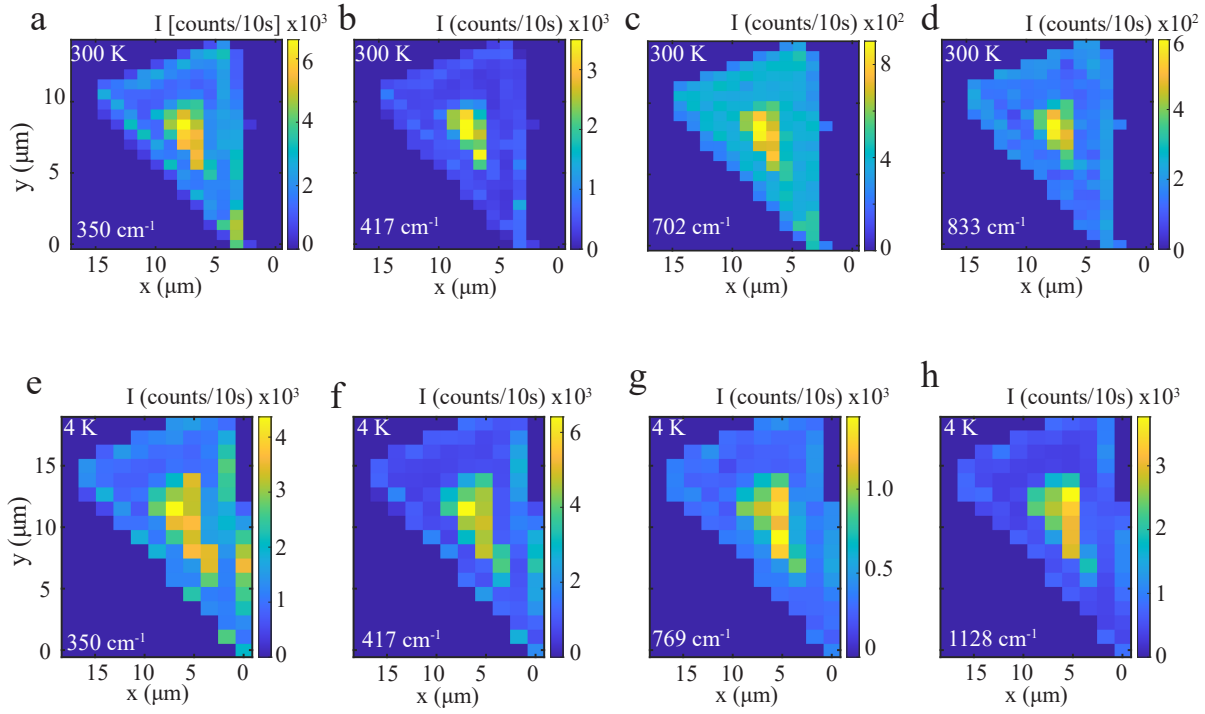

FIG. 4. **Position dependence of Raman intensity**
a-d Intensity map of the Raman features of the hollow WS_2 pyramid **a.** around 350 cm^{-1} (2LA,E_{2g}), **b.** around 417 cm^{-1} (A_{1g}), **c.** around 702 cm^{-1} (4LA) and **d.** around 833 cm^{-1} ($2A_{1g}$), taken at room temperature upon a 561 nm excitation. **e-h** Intensity map of the Raman features of the hollow WS_2 pyramid **e.** around 350 cm^{-1} (2LA,E_{2g}), **f.** around 417 cm^{-1} (A_{1g}), **g.** around 770 cm^{-1} (A_{1g}+2LA) and **h.** around 1120 cm^{-1} (6LA), taken at 4 K upon a 561 nm excitation. Note that in all cases (compare with Fig.4a,b in the main text) the intensity of the Raman features from the pyramid crater is significantly higher than the Raman intensity from the stair-like sides.

III. SPECTRAL FEATURES OF PYRAMIDS, MONOLAYER AND FEW-LAYER WS_2

Figure 4 presents maps of the intensity of different Raman features in spectra from the hollow WS_2 pyramid, taken at room temperature (Fig.4a-d) and at 4 K (Fig.4e-h) upon a 561 nm excitation. Note that for all the Raman features the intensity from the pyramid crater is higher than from the pyramid sides, as was the case for the Raman features depicted in Fig.4a,b in the main text (595 nm excitation, 200 K). We conclude that the intensity distribution of the Raman features is independent of temperature or excitation frequency. As alluded to in the main text, we hypothesise that light scatters from the stair-like pyramid sides and thus reduces the available excitation light to excite any Raman modes, or that scattering of the resulting Raman response reduces the amount of light detected.

Figure 3g depicts a comparison between the spectral response of the pyramid (in orange) and five layers of exfoliated WS_2 (in blue) at 4 K and upon a 595 nm excitation. The spectral response of the few-layer WS_2 exhibits a combination of Raman modes and PL from the excitonic resonance. Due to the high PL intensity, the higher-order Raman modes are much less clear in the few-layer WS_2 than in the pyramid spectrum. In both spectra, the A_{1g} mode has a higher intensity than the E_{2g} mode. The ratio of E_{2g}/A_{1g} is 0.60 for few-layer WS_2, whereas it is on average 0.79 for the pyramid spectra (see Fig.6b in the main text).

Figure 5a-c present room-temperature maps of the ratio between the first two Raman peaks in the spectra (E_{2g}/A_{1g}) of respectively the WS_2 monolayer, the hollow pyramid and a full WS_2 pyramid (compare the presented SEM images). In contrast with the position dependent peak ratio of the hollow pyramids, the peak ratio on the monolayer is homogeneous along the full flake (see Fig.5a). This ratio is around 1.4, as can be observed in the Raman spectrum in Fig.5d. The Raman peak ratio of the hollow pyramids upon 561 nm excitation is much higher on the pyramid sides than in the pyramid crater

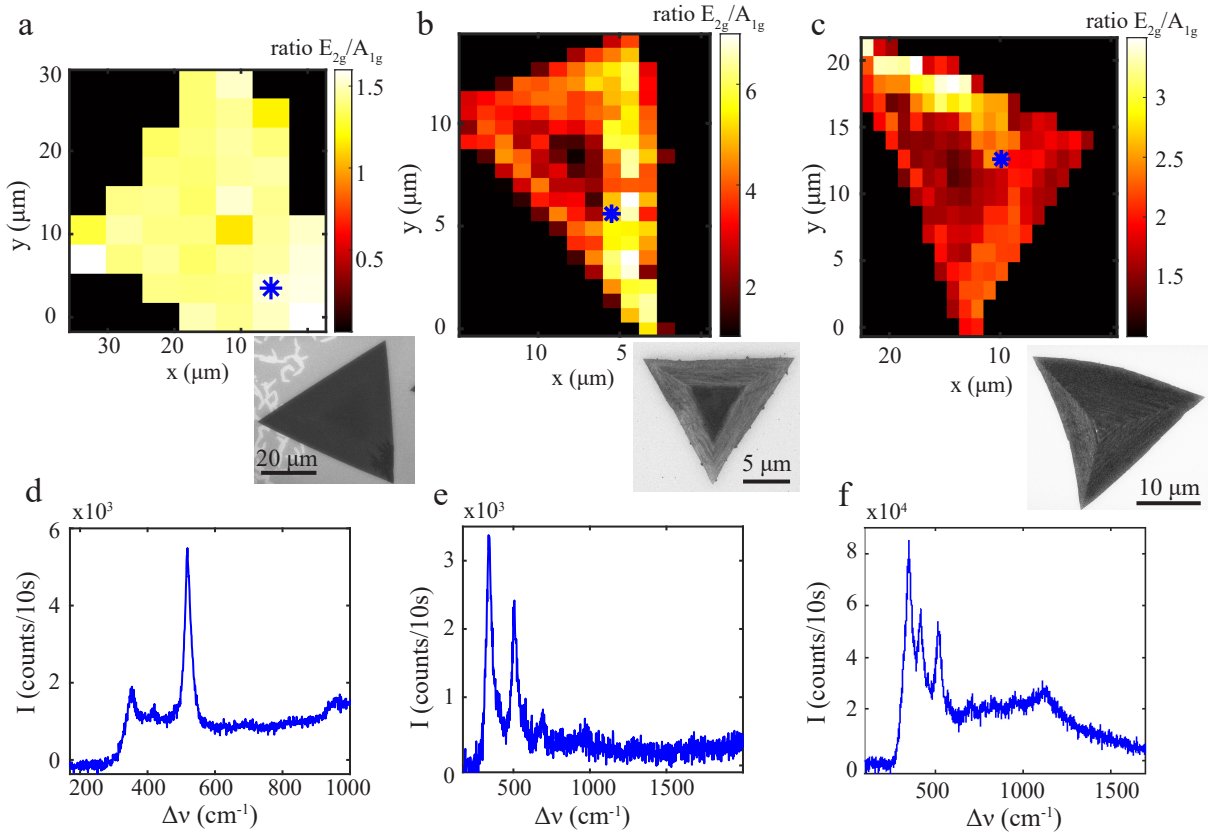

FIG. 5. **Position dependence of peak ratio**
a-c Room-temperature map of the ratio between the first two Raman features in the spectra (E_{2g}/A_{1g}) of **a** the monolayer, **b** the hollow pyramid and **c** a full WS_2 pyramid (compare SEM images) (blue stars indicate the positions of the spectra in **d-f**). **a.** The peak ratio on the monolayer is homogeneous along the full flake, 1.4 on average (upon a 561 nm excitation). **b.** The peak ratio on the hollow pyramid (upon a 561 nm excitation) is much higher along the stair-like pyramid sides (namely 4-7) than on the pyramid crater (roughly 1.0). **c.** The peak ratio on the full pyramid is significantly higher along the upper side. Note in the presented SEM image that this side of this full WS_2 pyramid is curved, potentially inducing strain. **d.** Raman spectrum of the WS_2 monolayer. **e.** Spectrum of the side of the WS_2 hollow pyramid upon 561 nm excitation. Note that the A_{1g} feature is merely a shoulder on the E_{2g},2LA(M) feature, which explains the high peak ratio in **b**. **f.** Spectrum of the full WS_2 pyramid (595 nm excitation), which is comparable to the spectra of the hollow WS_2 pyramid presented in the main text.

(see Fig.5b). This difference in ratio was already apparent upon 595 nm excitation, as presented in Fig.4f in the main text, but the contrast between the pyramid sides and crater is much larger upon 561 nm excitation. The Raman peak ratio at the pyramid sides is as high as 4-7 times, as the A_{1g} feature is reduced to merely a shoulder on the E_{2g},2LA(M) feature. This becomes apparent in the spectrum in Fig.5e. The SEM image under Fig.5c depicts a full WS_2 pyramid grown on the same substrate. This pyramid exhibits a clear curvature. Interestingly, the Raman peak ratio of the spectra from this pyramid (upon a 595 nm excitation) exhibit a difference on the side with the largest curvature, potentially induced by strain. Figure 5f presents a spectrum of the full WS_2 pyramid, which is similar to the spectra of the hollow WS_2 pyramid in the main text. We conclude that the Raman peak ratio provides information on differences in the atomic structure between different nanostructures, as well information on differences in both atomic structure and strain or stress within the same nanostructure.

Another position-dependent spectral feature alluded to in the main text is the spectral position of the Raman peaks. Figure 6 presents a map of the spectral position of the first Raman peak on the WS_2 monolayer and the full WS_2 pyramid respectively. The peak position is fairly homogeneous along both nanostructures compared to the hollow pyramid (Fig.5a in the main text). Figure 6c depicts the average spectral position of the first Raman peak, as measured on different WS_2 pyramids and the monolayer (the bar does not indicate errors, but rather the spread of the peak position along the pyramids). The peak position on the monolayer is around 357 cm^{-1}, which is significantly different than the peak position of around 350 cm^{-1} on all the pyramid

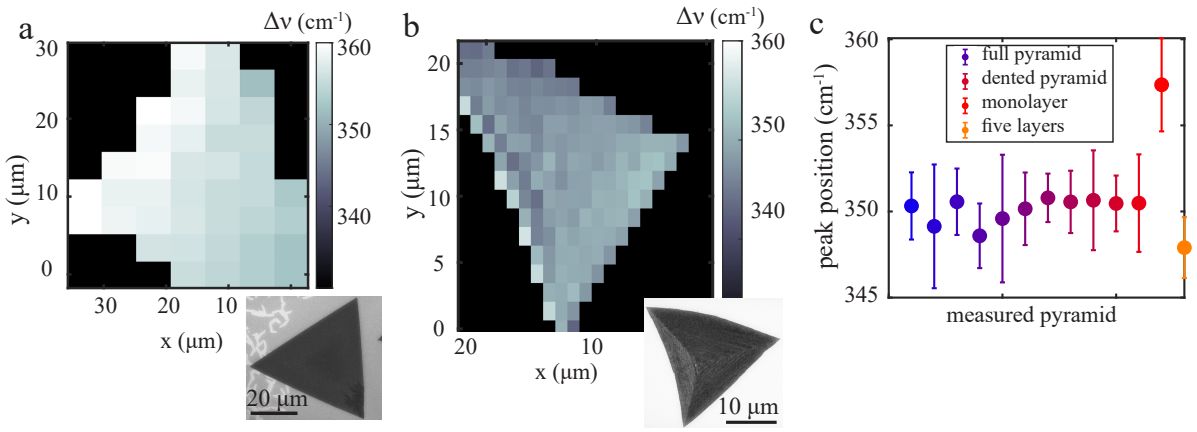

FIG. 6. **Position dependence of spectral position**
a-b Room temperature map of the first WS_2 Raman feature around 350cm^{-1} on **a** the monolayer and **b** a full WS_2 pyramid (compare SEM images). Comparing **a** and **b** and Fig.5 in the main text, it becomes apparent that the Raman peak position on the monolayer is significantly different than on the pyramids. **c** depicts the average spectral position of the first Raman peak on all measured pyramids and the monolayer. Note that the bar does not indicate errors, but rather the spread of the peak position along the pyramids. The first Raman feature on the monolayer is around 357 cm^{-1}, whereas on all measured pyramids, it is around 350 cm^{-1}, and around 348 cm^{-1} on five layers of WS_2. Possibly this Raman peak has a larger contribution from the E_{2g} than the 2LA(M) phonon in the monolayer than in the pyramid spectra.

structures and 348 cm^{-1} for five layers of exfoliated WS_2. We hypothesise that this first Raman peak has a larger contribution from the E_{2g} than the 2LA(M) phonon in the monolayer than in the pyramid spectra. In conclusion, the different nanogeometry of the WS_2 pyramids induces spectral changes with respect to monolayer WS_2.

IV. STRUCTURAL CHARACTERISATION

Figure 7 displays additional results obtained in the structural characterization measurements by means of Transmission Electron Microscopy (TEM). Figure 7a presents a high-resolution ADF-STEM image taken at the side of a hollow WS_2 pyramid. Within Figure 2 of the main text it could already be observed that the atomic arrangements present in the sides of the WS_2 pyramid and the middle are not the same. Figure 7a depicts how even within a given region the atomic arrangement can vary. This is highlighted by the differences in the FFTs taken in the lower left corner (marked by the green rectangle in Fig.7a) and the top right corner (marked by the blue rectangle in Fig.7b) of this given region. Where the FFT in the blue area shows two nicely arranged hexagonal patterns, *e.g.*, an inner and an outer hexagon, the green area presents one hexagon. These subtle variations of the atomic arrangement might be induced by the local presence of strain, which in turn results into a slight change of the orientation of the flake.

Figures 7b to 7d depict low-magnification ADF images of the hollow WS_2 pyramid. Within Fig.7b the hollow nature of the pyramid can clearly be observed, and illustrated even clearer in the line profile taken along the white line given in Fig.7b. In addition, Fig.7b-d depict how free-standing WS_2 flakes seem to arise from the walls of the hollow pyramid. These increase the level of structural disorder in the middle of the pyramids as compared to the sides. The standing flake depicted in the low-magnification ADF image of Fig.7d highlights the possible growth mechanism leading to the hollow WS_2 pyramids. In this figure it can be observed that both layer-by-layer stacking and screw-dislocation-driven growth mechanisms contribute to the overall growth mechanism of the hollow WS_2 pyramids.

[1] Kin Fai Mak, Changgu Lee, James Hone, Jie Shan, and Tony F. Heinz. Atomically thin mos2: A new direct-gap semiconductor. *PRL*, 105(13):136805, September 2010.
[2] Su-Hyun Gong, Filippo Alpeggiani, Beniamino Sciacca, Erik C. Garnett, and L. Kuipers. Nanoscale chiral valley-photon interface through optical spin-orbit coupling. *Science*, 359(6374):443–447, 2018.
[3] Maciej R. Molas, Karol Nogajewski, Artur O. Slobodeniuk, Johannes Binder, Miroslav Bartos, and Marek Potemski. The optical response of monolayer, few-layer and bulk tungsten disulfide. *Nanoscale*, 9(35):13128–13141, 2017.
[4] Weijie Zhao, R. M. Ribeiro, Minglin Toh, Alexandra Carvalho, Christian Kloc, A. H. Castro Neto, and Goki Eda. Origin of indirect optical transitions in few-layer mos2, ws2, and wse2. *Nano Lett.*, 13(11):5627–5634, November

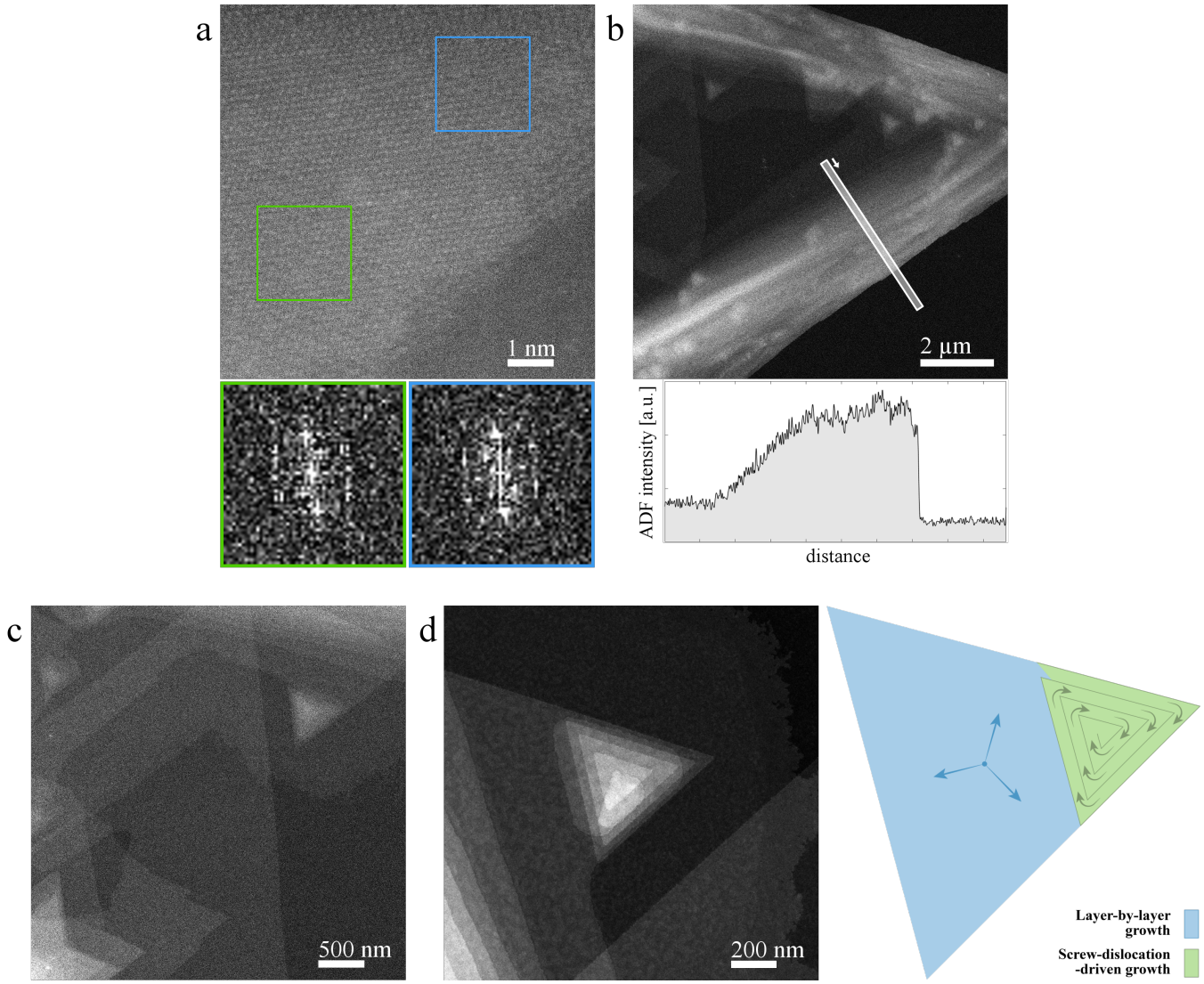

FIG. 7. **ADF-STEM of a hollow WS_2 pyramid**
a. Atomic resolution ADF-STEM image taken at the side of a hollow WS_2 pyramid. **inset** FFTs are taken within two visual different areas of this given region, highlighting a clear difference between the two areas. **b-d.** Low-magnification ADF images of the same hollow pyramid. The characteristic morphology of the hollow pyramids can clearly be observed, and is also extracted from the line profile over the white line given within **b** (see inset). Each of these images show free-standing flakes which arise from the walls of the hollow pyramid. The free-standing flake shown in **d** suggest a growth mechanism where layer-by-layer stacking and screw-dislocation-driven growth mechanisms co-exist. **inset** A schematic visualises this co-existence. Here a free-standing flake initiates its growing from a central nucleation point via layer-by-layer growth (blue), after which a separate nucleation event occurs leading to a screw-dislocation-driven growth (green) on top.

2013.
[5] Gerd Plechinger, Philipp Nagler, Julia Kraus, Nicola Paradiso, Christoph Strunk, Christian Schüller, and Tobias Korn. Identification of excitons, trions and biexcitons in single-layer ws2. *Phys. Status Solidi RRL*, 9(8):457–461, August 2015.
[6] Toshiaki Kato and Toshiro Kaneko. Transport dynamics of neutral excitons and trions in monolayer ws2. *ACS Nano*, 10(10):9687–9694, October 2016.
[7] J. Jadczak, J. Kutrowska-Girzycka, P. Kapuściński, Y. S. Huang, A. Wójs, and L. Bryja. Probing of free and localized excitons and trions in atomically thin wse2, ws2, mose2 and mos2 in photoluminescence and reflectivity experiments. *Nanotechnology*, 28(39):395702, 2017.
[8] Zhengyu He, Xiaochen Wang, Wenshuo Xu, Yingqiu Zhou, Yuewen Sheng, Youmin Rong, Jason M. Smith, and Jamie H. Warner. Revealing defect-state photoluminescence in monolayer ws2 by cryogenic laser processing. *ACS Nano*, 10(6):5847–5855, June 2016.